THE JOURNAL OF BIOLOGICAL CHEMISTRY VOL. 287, NO. 3, pp. 1755–1769, January 13, 2012
© 2012 by The American Society for Biochemistry and Molecular Biology, Inc. Published in the U.S.A.

Alternative Splicing Regulates Kv3.1 Polarized Targeting to Adjust Maximal Spiking Frequency*[S]

Received for publication, August 30, 2011, and in revised form, November 9, 2011 Published, JBC Papers in Press, November 21, 2011, DOI 10.1074/jbc.M111.299305

Yuanzheng Gu[‡], Joshua Barry[§], Robert McDougel[¶], David Terman[¶], and Chen Gu[‡§1]

From the [‡]Department of Neuroscience and Center for Molecular Neurobiology, [§]Molecular, Cellular and Developmental Biology Graduate Program, and the [¶]Department of Mathematics, The Ohio State University, Columbus, Ohio 43210

Background: Ion channels play critical roles in converting synaptic inputs into digital outputs encoded by action potentials.
Results: Kv3.1 axonal targeting, regulated by its C-terminal splice domain, enhances the maximal spiking frequency.
Conclusion: Channel biophysical properties and localization are both important for Kv3.1-mediated fast spiking in neurons.
Significance: This is the first report showing an important function of polarized targeting of Kv channels.

Synaptic inputs received at dendrites are converted into digital outputs encoded by action potentials generated at the axon initial segment in most neurons. Here, we report that alternative splicing regulates polarized targeting of Kv3.1 voltage-gated potassium (Kv) channels to adjust the input-output relationship. The spiking frequency of cultured hippocampal neurons correlated with the level of endogenous Kv3 channels. Expression of axonal Kv3.1b, the longer form of Kv3.1 splice variants, effectively converted slow-spiking young neurons to fast-spiking ones; this was not the case for Kv1.2 or Kv4.2 channel constructs. Despite having identical biophysical properties as Kv3.1b, dendritic Kv3.1a was significantly less effective at increasing the maximal firing frequency. This suggests a possible role of channel targeting in regulating spiking frequency. Mutagenesis studies suggest the electrostatic repulsion between the Kv3.1b N/C termini, created by its C-terminal splice domain, unmasks the Kv3.1b axonal targeting motif. Kv3.1b axonal targeting increased the maximal spiking frequency in response to prolonged depolarization. This finding was further supported by the results of local application of channel blockers and computer simulations. Taken together, our studies have demonstrated that alternative splicing controls neuronal firing rates by regulating the polarized targeting of Kv3.1 channels.

The ability of a neuron to integrate synaptic inputs and generate proper action potential (AP)[2]-encoded outputs relies on the concerted actions of ligand- and voltage-gated ion channels that are present on its plasma membrane. Most neurons have multiple dendrites and one long axon, important for the neuronal input and output functions, respectively. Various types of Kv channels, with distinct biophysical and pharmacological properties, are differentially localized in dendrites and the axon. In mammalian brains, Kv1 (*Shaker*) channels are predominantly distributed along axons, whereas Kv2 (*Shab*) and Kv4 (*Shal*) channels are mainly localized in dendritic regions (1–10). Kv3 (*Shaw*) channels display complex targeting patterns. Depending on the isoform, alternative splicing, and neuronal types, some Kv3 channels localize in axons and some in dendrites (11–19). Progress has been made in identifying molecular mechanisms underlying polarized targeting of different Kv channels (16, 20–25). However, the exact function of the regulation of polarized targeting of Kv channels remains a mystery.

Excitatory and inhibitory synaptic potentials generated in dendrites and soma are summed and converted into one or a number of APs at the AIS of most neurons, where voltage-gated sodium (NaV) channels are highly concentrated. The AIS is also critical for gating the entry of axonal proteins (26, 27). The spiking frequency of each neuron must properly reflect the strength of synaptic potentials. Regulation of the input-output relationship, which is emerging as a new form of plasticity of intrinsic excitability, is still poorly understood. The widest range of spiking frequencies is usually attributable to the presence of Kv3 channels, because of their unique biophysical properties, high activation threshold (about −20 mV), and rapid deactivation kinetics (28, 29). However, it remains unknown whether Kv3 channel expression is sufficient for fast spiking, because not all Kv3-expressing neurons spike rapidly (11). This raises an intriguing question: how does the polarized targeting of Kv3 channels regulate the spiking frequency?

In this study, we use hippocampal neurons as a model system (30–32) to examine how Kv3-polarized targeting affects the neuronal input-output relationship. Our results show that besides their essential role in increasing AP firing frequency, the expression of axonal Kv3.1b channels is sufficient to convert a slow-spiking young neuron to a fast-spiking one. Interestingly, the increase of an outward K^+ current actually enhances neuronal excitability reflected by increased AP firing frequency. Moreover, our mutagenesis studies reveal novel mechanistic insights into axonal targeting of Kv3.1b. Our stud-

* This work was supported, in whole or in part, by National Institutes of Health Grant R01NS062720 from the NINDS (to C. G.) and National Science Foundation Grant DMS-1022627 (to D. T.). All animal experiments have been conducted in accordance with the National Institutes of Health Animal Use Guidelines.

[S] This article contains supplemental Figs. S1–S9.

[1] To whom correspondence should be addressed: 182 Rightmire Hall, 1060 Carmack Rd., Columbus, OH 43210. Tel.: 614-292-0349; Fax: 614-292-5379; E-mail: gu.49@osu.edu.

[2] The abbreviations used are: AP, action potential; Kv channel, voltage-gated potassium channel; AIS, axon initial segment; NaV channel, voltage-gated sodium channel; DIV, day *in vitro*; TEA, tetraethylammonium; ATM, axonal targeting motif; E18, embryonic day 18; P8, postnatal day 8.

ies suggest that axon-dendrite targeting of Kv3.1 channels can effectively adjust the maximal spiking frequency.

EXPERIMENTAL PROCEDURES

cDNA Constructs—Kv3.1aHA, Kv3.1bHA, Kv3.1bHA$_{1-502}$, YFP-Kv1.2, and Kvβ2 were previously described (16, 21). YFP-Kv4.2 was made by inserting a cDNA fragment encoding YFP into the N terminus of Kv4.2 before its T1 domain between SalI and NheI restriction enzyme sites, which were engineered between the codons for Lys[36] and Arg[37] using the QuikChange mutagenesis strategy. Kv3.1bHA$_{1-513}$, Kv3.1bHA$_{1-530}$, and Kv3.1bHA$_{1-554}$, were made by engineering stop codons in Kv3.1bHA C terminus with QuikChange mutagenesis. Kv3.1bHA$_{DE-KK}$, Kv3.1bHA$_{ED-AA}$, Kv3.1bHA$_{ED-KK}$, and Kv3.1bHA$_{ED-AA}$ were made with QuikChange mutagenesis.

Hippocampal Neuron Cultures and Transfection—The E18 hippocampal neuron culture was prepared as previously described from rat hippocampi at the embryonic day 18 (E18) (16, 23). In brief, 2 days after neuron plating, 1 μM cytosine arabinose (Ara-C, Sigma) was added to the neuronal culture medium to inhibit glial growth for the subsequent 2 days, then replaced with normal culture medium. The culture medium was replenished twice a week by replacing half the volume. For transient transfection, neurons in culture at 5–7 DIV (day *in vitro*) were incubated in Opti-MEM containing 0.8 μg of cDNA plasmid and 1.5 μl of Lipofectamine 2000 (Invitrogen) for 20 min at 37 °C. At least three independent transfections were performed for each condition.

The P8 hippocampal neuron culture was prepared from rat hippocampi at postnatal day 8 (P8) to obtain interneuron-enriched cultures, using the same procedure as the E18 culture as described previously (23). Enrichment of GABAergic interneurons in P8 cultures may reflect differences in the birth and migration of GABAergic interneurons *versus* pyramidal neurons. In addition, pyramidal neurons may die more readily during dissociation for culture, because P8 pyramidal neurons already have lengthy and complex dendritic and axonal arbors. Neurons were usually cultured for about 14 to 21 DIV before the experiments.

Voltage Clamp Recording to Determine Channel Biophysical Properties—Biophysical properties of various Kv channel constructs were determined by voltage clamp recording studies on transfected HEK293 cells and neurons. HEK293 cells were maintained in cell line medium (minimum essential medium with 10% fetal bovine serum, 1 mM sodium pyruvate, 0.5 mM L-glutamine, and penicillin-streptomycin). They were transfected with Lipofectamine2000 using the same protocol as for cultured neurons. The transfected HEK293 cells were identified by fluorescence from co-transfected YFP. They were recorded in Hanks' buffer (150 mM NaCl, 4 mM KCl, 1.2 mM $MgCl_2$, 10 mg/ml of glucose, 1 mM $CaCl_2$, 20 mM HEPES (pH 7.4)). The internal solution of electrical pipettes was composed of (in mM) 122 $KMeSO_4$, 20 NaCl, 5 Mg-ATP, 0.3 GTP, and 10 HEPES (pH 7.2). The resistance of electrodes was between 2 and 5 MΩ. Whole cell voltage clamp recording was performed at room temperature (~25 °C) using an Axopatch 200B amplifier, a digidata 1440A, and pCLAMP10 software (Molecular Devices, Downingtown, PA). Currents were filtered at 5 kHz. Membrane potentials of isolated cells were normally held at −80 mV. Voltage pulses from −60 to +60 mV with 200–250-ms duration and 10-mV increments were applied.

Conductance-voltage relationships (G-V curves) for Kv channel constructs were: $G = I/(V_m - V_{rev})$, $V_{rev} = -95$ mV, normalized to the maximal conductance. Curves were fitted with Boltzmann function, $G/G_{max} = 1/(1 + \exp[-(V - V_{1/2})/k])$, where G_{max} is the maximal conductance, V is the membrane potential, $V_{1/2}$ is the potential at which the value of the relative conductance is 0.5, and k is the slope factor. SigmaPlot 10.0 (Systat Software, Inc., Chicago, IL) was used for fitting.

To obtain activation time constant (τ_{on}), activation curves (voltage was increased from −80 to +30 mV) were fitted with a single exponential function raised to a power of 4, $I(t) = A(1 - \exp(-t/\tau_{on}))^4$. In studies of deactivation kinetics of Kv channels, the cells were held at −80 mV, given a 2-ms pre-pulse to +60 mV and 20-ms voltage pulses from −100 to −10 mV. To obtain deactivation time constants (τ_{off}), tail currents (voltage decreasing from +60 to −60 mV) were fitted with the equation, $I(t) = A_{exp}(-t/\tau_{off})$. Clampfit 10.0 was used for fitting to get τ_{on} and τ_{off}.

Current Clamp Recording of Action Potentials—The same internal solution and Hanks' buffer were used for recording of primary cultured neurons. Both mature neurons (older than 16 DIV) and young neurons (7 to 10 DIV) were recorded from either the E18 or the P8 cultures. The membrane resistance, capacitance, and resting membrane potentials of the neurons were measured. These values are consistent within each age group. APs induced by either puffing (0.5–1 s in duration) 2 μM glutamate (Glu) onto neuronal soma, or current injection from the recording pipette, were recorded under the current clamp mode. For long pulse stimulations, 1000-ms duration currents of increasing amplitude (from 5 to 145 pA with increments of 10 pA) were injected. Due to the variation of expression levels of transfected channel constructs, only the neurons carrying clear after-hyperpolarization were used for quantification of spiking frequency. For short pulse stimulations, 2-ms duration currents of 800 pA with increasing frequency (from 50 to 300 Hz with increment of 50 Hz) were injected. Because the current injection is very short for short pulse stimulations, we found that only the large current (800 pA) can reliably induce the first AP in control neurons, consistent with previous studies (33–35).

Post Hoc Immunostaining of Hippocampal Neurons from P8 Culture—To examine the AP firing frequency of the endogenous Kv3.1 channels role, we performed current clamp recording on the P8 neurons from 14 to 16 DIV. For each neuron, induced AP traces by long-pulse stimulation were recorded and its morphology was imaged with transmitted light. The neuron was fixed immediately after recording, permeabilized with 0.2% Triton X-100, and stained for endogenous Kv3.1b and NaV channels with a mouse monoclonal anti-Kv3.1b antibody (clone number B16B/8; University of California Davis/NIH NeuroMab Facility, Davis, CA) and a rabbit polyclonal anti-pan NaV channel antibody (Millipore), respectively. The maximal AP frequency and immunostaining intensity of endogenous Kv3.1b in proximal axons are correlated.

Local Drug Application and Effects on Action Potential Firing—Glass pipettes with a tip diameter around 1 μm for patch clamp

recording were pulled with a model P-1000 Flaming/Brown micropipette puller (Sutter Instrument, Novato, CA). Glass pipettes with diameters around 50 μm, made by adjusting the pulling parameters and filled with either 2 μM Glu or 1 mM tetraethylammonium (TEA), were used for perfusion of whole neurons. Glass pipettes with diameters around 3 μm, pulled with a designated program and filled with 1 mM TEA, were used for local perfusion onto axons or dendrites.

Immunostaining, Imaging, and Quantification—The immunocytochemical procedures were previously described (16, 21). Briefly, neurons were stained under nonpermeabilized conditions (without Triton X-100) to label the surface pool and under permeabilized conditions (with 0.2% Triton X-100) to label total proteins. Fluorescence images were captured with a Spot CCD camera RT slider (Diagnostic Instrument Inc., Sterling Heights, MI) in a Zeiss upright microscope, Axiophot, using Plan Apo objectives ×20/0.75 and ×100/1.4 oil, saved as 16-bit TIFF files, and analyzed with NIH ImageJ and Sigmaplot 10.0 for fluorescence intensity quantification. Exposure times were controlled so that the pixel intensities in dendrites and axons were below saturation, but the same exposure time was used within each group of an experiment. The quantification procedure was described previously (16, 23). Only transfected neurons with clearly separated dendrites and axons, and isolated from other transfected cells, were chosen for analysis. To obtain the axonal polarity index (F_{axon}/F_{dend}) reflecting polarized targeting on the neuronal surface, we performed anti-HA staining under the nonpermeabilized condition. Using NIH ImageJ, we laid a line along the major axon to acquire its average fluorescence intensity (in arbitrary unit) (F_{axon}), and laid lines along proximal dendrites 10 μm away from the soma to obtain the average fluorescence intensity on dendritic membranes (F_{dend}). To obtain the relative axonal level of total proteins (F_{axon}/F_{sd}), we performed anti-HA staining under permeabilized conditions. Using NIH ImageJ, we laid a line along the major axon to acquire F_{axon}, and laid lines along proximal dendrites starting from the soma to obtain F_{sd}. The background fluorescence intensity was measured for each image and subtracted.

Simulation of Action Potential Firing Using NEURON Software—The computation model was implemented using NEURON 7.1 (36). We assumed a simplified morphology, largely consistent with a cultured hippocampal neuron at 10 DIV. The cell was constructed using three cylinders, each representing a distinct region of the neuron: a dendrite (100 μm in length and 4 μm in diameter), a soma (20 μm in length and 20 μm in diameter), and an axon (400 μm in length and 2 μm in diameter). The AIS is located in the first 10–45 μm of the axon.

Each simulation was compared three model neurons (control, dendritic Kv3.1, and axonal Kv3.1) with different Kv3 channel distributions but otherwise identical, that is, they had the same morphology, NaV channel distribution, and leak channel distribution.

In dendritic Kv3.1-expressing neurons, Kv3 current density is relatively higher on the somatodendritic surface, whereas in axonal Kv3.1-expressing neurons, Kv3 current density is relatively higher on the axonal surface including the AIS. This is largely consistent with the immunostaining results under the nonpermeabilized condition.

In Fig. 8, *A* and *B*, we provide one example of the simulation results. The parameters used in this figure are as follows: NaV channels carrying transient Na^+ currents were present throughout the cell, with density in the AIS (37,300 pS/μm^2) five times higher than along the rest of the axon (7,460 pS/μm^2) and 20 times higher than the rest of the cell (1,865 pS/μm^2). In the control neuron, Kv3.1 channels were absent. In the dendritic Kv3.1-expressing neuron, Kv3.1 channels were present on somatic and dendritic membranes (20,000 pS/μm^2) and axonal membranes including the AIS (1,000 pS/μm^2). In the axonal Kv3.1-expressing neuron, Kv3.1 channels were present on somatic and dendritic membranes (5,000 pS/μm^2) and axonal membranes including the AIS (15,000 pS/μm^2). The ratios of Kv3.1 channels used here were adopted from the most highly polarized examples observed in our immunostaining results (F_{axon}/F_{dend}) under the nonpermeabilized condition. It was assumed here that the anti-HA immunofluorescence signal is in a linear relationship with the actual amount of Kv3.1 channels. Leaky channel conductance was present throughout the cell at 7.1 pS/μm^2.

The biophysical properties of NaV channels, Kv3.1 channels, and leaky channels used in our model cells were adopted from Golomb *et al.* (37) with modifications based on experimentally observed time constants. The current balance equation is,

$$CV_t = (r/2R_a)V_{xx} - I_{Na}(V,h,x) - I_{Kv3}(V,n,x) - I_t(V) + I_{app} \quad \text{(Eq. 1)}$$

where V is the membrane potential of the neuron, $C = 1$ $\mu F/cm^2$ is the membrane capacitance, r is the section radius, $R_a = 35.4$ Ω-cm is the cytoplasmic resistivity, I_{app} denotes external current injected into the neurons, and I_{Na}, I_{Kv3}, and I_l represent the sodium (NaV), potassium (Kv3.1), and leak currents, respectively. These are modeled as: $I_{Na}(V,h,x) = g_{Na}(x)\, m_\infty^3(V)h(V - V_{Na})$; $I_{Kv3}(V,n,x) = g_k(x)n^2(V - V_K)$; and $I_l(V) = g_l(V - V_l)$, where $g_{Na}(x)$, $g_K(x)$, and g_l represent the maximum NaV, Kv3.1, and leak conductances, the first two vary with space depending on the region of the cell. The sodium, potassium, and leak reversal potentials are $V_{Na} = 50$ mV, $V_K = -77$ mV, and $V_l = -70$ mV, respectively.

Sodium activation is assumed to be instantaneous and is given by: $m_\infty(V) = 1/(1 + \exp(-(V - \theta_m)/\sigma_m))$. The sodium inactivation variable h are governed by,

$$h_t = (h_\infty(V) - h)/\tau_h(V) \quad \text{(Eq. 2)}$$

where $h_\infty(V) = 1/(1 + exp(-(V - \theta_h)/\sigma_h))$ and $\tau_h(V) = \phi_h (0.5 + 10/(1 + \exp(-(V - \theta_{th})/\sigma_{th})))$. We take $\theta_m = -24$ mV, $\sigma_m = 11.5$ mV, $\theta_h = -58.3$ mV, $\sigma_h = -6.7$ mV, $\theta_{th} = -16$ mV, $\sigma_{th} = -12$ mV, and $\phi_h = 1.5$.

The potassium activation variable n is governed by,

$$n_t = (n_\infty(V) - n)/\tau_n(V) \quad \text{(Eq. 3)}$$

where $n_\infty(V) = 1/(1 + \exp(-(V - \theta_{hn})/\sigma_n))$ and $\tau_h(V) = \phi_n (0.2 + 11.4/(1 + \exp((V + 3)/6)))(0.07 + 11.4/(1 + \exp(-(V - 1.3)/15)))$. We take $\theta_{hn} = -12.4$ mV, $\sigma_n = 6.8$ mV, and $\phi_h = 0.5$.

Long pulse experiments were performed as follows. First we administered a current at the midpoint of the soma for 5 s; then

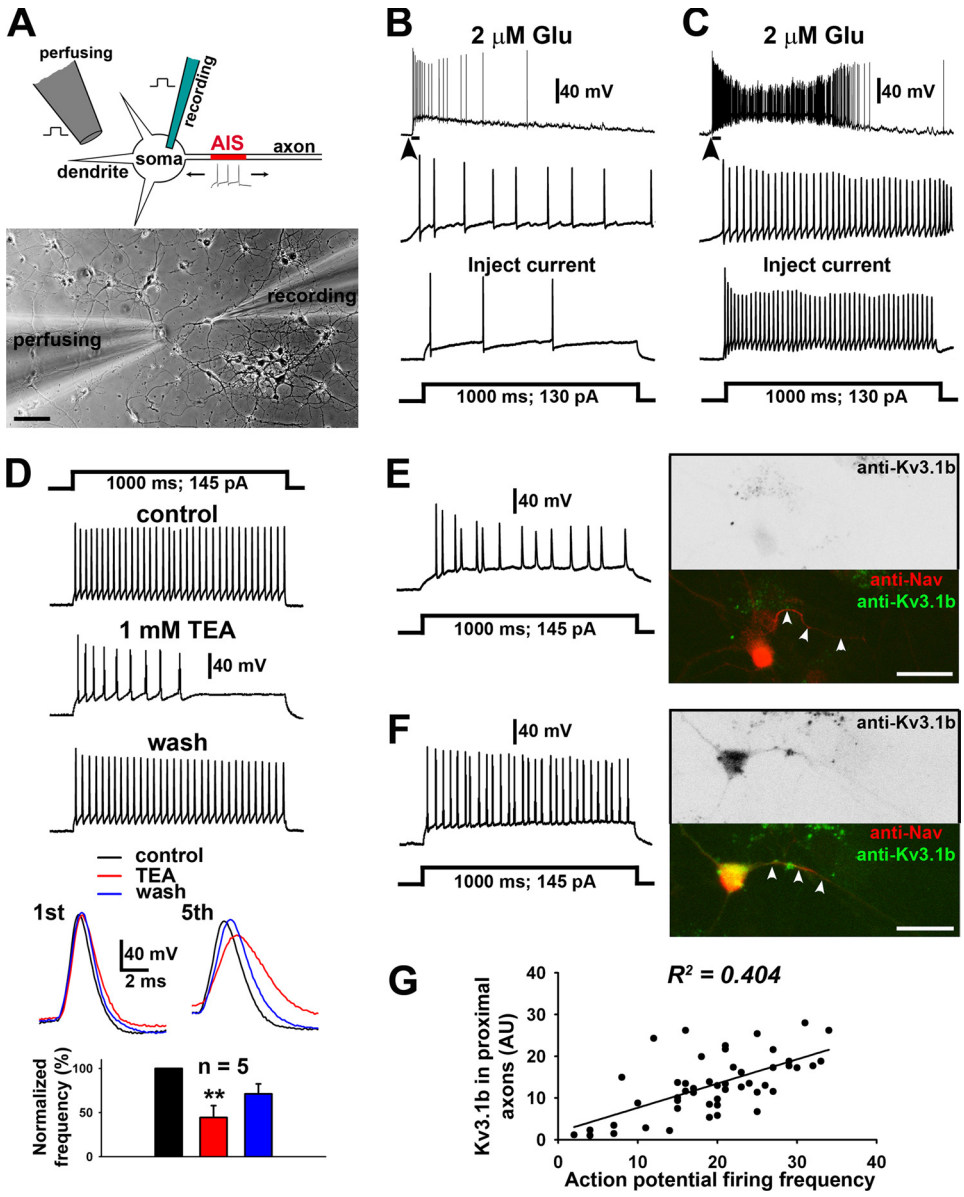

FIGURE 1. **Hippocampal neurons in culture spikes at different frequencies in response to prolonged depolarizing inputs.** *A,* whole cell current-clamp recording on cultured hippocampal neurons. In the experimental diagram of the whole cell recording of a cultured hippocampal neuron (*top*), a recording electrode (*green*) records membrane potentials and injects currents to induce APs. A drug perfusion pipette (*gray*) is used to apply either glutamate (Glu) or TEA to the neuron. Current injection and Glu puffing mimic presynaptic excitatory inputs to induce APs initiated at the AIS (*red*). APs propagate anterogradely along axons toward axonal terminals, and retrogradely back to soma picked up by the recording electrode. The *lower panel* shows a transmitted light image of the recoding of cultured hippocampal neurons at 14 DIV. *B*, a slow-spiking neuron firing APs induced by either a puffing (0.5–1 s) of 2 μM Glu (*upper*) or 1-s injection of 130 pA currents (*lower*). Recording of APs for 20 s is shown on the *top*, below which is the trace within the first 1 s of drug application. Neurons around 15 to 17 DIV from the P8 culture were used. *C*, a fast-spiking neuron firing APs induced by either Glu puffing (*upper*) or current injection (*lower*). *Black arrowheads* indicate the Glu puffing. *D*, fast spiking of cultured hippocampal neurons was reversibly blocked by perfusing 1 mM TEA. The first (*left*) and fifth (*right*) APs are shown. Summary of the result is at the *bottom*. Normalized frequency equals to AP frequency divided by the frequency under the control condition. Paired *t* test, **, $p < 0.01$. *E*, AP firing induced by 1-s current injection (*left*) and axonal levels of endogenous Kv3.1b (*right*) in a slow-spiking neuron. After recording, the neuron was fixed post hoc, and co-stained with anti-Kv3.1b (*green*) and anti-pan-NaV (*red*) antibodies. The anti-Kv3.1b staining is shown in reversed signal (*right top*). *F*, AP firing induced by 1-s current injection (*left*) and axonal levels of endogenous Kv3.1b (*right*) in a neuron firing more rapidly. *White arrowheads* indicate proximal axons. *G*, summary of the correlation of axonal Kv3.1b levels and AP frequencies. Pearson test, $p < 0.0001$. $n = 49$. *Scale bars*, 100 μm in *A* and 50 μm in *E* and *F*.

we counted the number of spikes; and finally divided the total count by 5 to get the firing rate. We established the robustness of the qualitative result that axonal Kv3.1 leads to a higher firing rate than dendritic Kv3.1 by keeping the expression ratios constant and randomly choosing base conductances in the following ranges: g_{Na} (peak expression) between 0 and 50,000 pS/μm^2, g_K (lowest expression) between 0 and 10,000 pS/μm^2, and g_l between 0 and 20 pS/μm^2.

RESULTS

Spiking Frequency of Hippocampal Neurons and Endogenous Kv3 Channels—To determine AP firing patterns of various mature hippocampal neurons (from 16 to 28 DIV), we performed whole cell current-clamp recordings on neurons from the E18 and P8 cultures (Fig. 1*A*). To mimic excitatory inputs, 2 μM Glu was puffed (0.5–1 s) onto neuronal dendrites and soma.

Glu puffing depolarized the membrane potential and induced AP firing (Fig. 1, *B* and *C*). In the same neuron, we also injected square-wave current pulses into the soma to induce APs. Similar spiking frequency resulted from the two different induction methods. In a slow-spiking neuron, Glu puffing and current injection led to a few APs per second (Fig. 1*B*). In contrast, in a fast-spiking like neuron, both Glu puffing and current injection induced much higher firing rates (Fig. 1*C*). Our finding that these cultured neurons display a variety of spiking frequencies is consistent with the fact that the hippocampus contains different types of neurons with distinct firing properties, including fast-spiking, parvalbumin-positive GABAergic interneurons (38).

To determine the role of Kv3 channels in regulating the spiking frequency, we examined the effect of a low concentration (1 mM) TEA, which preferentially blocks Kv3 channels (28). Indeed, the fast spiking of recorded neurons were markedly and reversibly suppressed by 1 mM TEA (normalized frequency control, 100%; 1 mM TEA, 44.4 ± 13.4%; wash, 71.1 ± 11.3%; $n = 5$) (Fig. 1*D*). Before TEA application, these neurons exhibited spiking patterns that are characteristic of fast-spiking neurons, which are nearly constant AP amplitudes, uniform interspike intervals, and high firing frequencies (Fig. 1*D*). The TEA application broadened AP duration; this was especially prominent in subsequent APs (Fig. 1*D*). Due to broadening of the duration of previous APs, initiation of the 5th AP was much delayed and its amplitude also decreased (Fig. 1*D*). However, it is important to note that TEA does block other Kv channels at 1 mM concentration, although with less efficacy compared with Kv3.

To further examine the potential role of Kv3.1 channels, we combined the current-clamp recording with post hoc immunostaining. Neurons were imaged with transmitted light during recording, immediately fixed afterward, and stained for endogenous Kv3.1b and NaV channels. A slow-spiking neuron often did not express any Kv3.1b at all (Fig. 1*E*), whereas a fast-spiking neuron expressed endogenous Kv3.1b in neuronal soma and proximal axons (Fig. 1*F*). Expression levels of Kv3.1b along proximal axons correlate with the maximal spiking frequency (Fig. 1*G*). Overall, the percentage of fast-spiking-like neurons was low (fast, ~11%, >31 Hz; medium ~28%, 21–30 Hz; slow, ~61%, <20 Hz; $n = 218$), consistent with the staining result. Taken together, our study is consistent with the notion that Kv3 channels play a critical role in generating fast spiking within neurons (28).

Expression of Kv3.1b Effectively Converts Slow-spiking Young Neurons into Fast-spiking Neurons—Next, we examined whether Kv3 expression is sufficient to induce fast spiking by using hippocampal neurons from the E18 culture. At different developmental stages (from 4 to 22 DIV), there was maturation of neuron morphology, with increased axonal and dendritic length and branching patterns (supplemental Fig. S1). This was accompanied by APs displaying increased amplitude and shortened duration (supplemental Fig. S1), which is consistent with the AP maturation revealed from *Xenopus* spinal neurons and rodent auditory neurons, where increased expression of NaV and Kv channels plays a major role (39–42). We transfected various Kv channel constructs into neurons at 5 DIV and then recorded them from 7 to 10 DIV. This is because there were sufficient NaV channels (supplemental Fig. S2). On the other hand, the expression levels of endogenous Kv channels is low and the outward currents increased by over 5-fold when Kv3.1 was transfected (control, 1.56 ± 0.22 nA, $n = 10$; Kv3.1aHA, 11.43 ± 1.09 nA, $n = 10$; Kv3.1bHA, 9.79 ± 0.60 nA, $n = 6$), rendering a relatively clean background (supplemental Fig. S2). Importantly, we have never observed fast spiking from these cultured neurons at this stage.

When expressed in the neurons, Kv3.1bHA markedly increased the maximal spiking frequency in response to prolonged current injections (1 s duration), effectively converting slow-spiking neurons to fast-spiking ones, firing APs up to 100 Hz (Fig. 2*A*). The firing pattern is characteristic of fast-spiking neurons with narrow spikes and rather constant amplitudes/inter-spike intervals. YFP-tagged Kv1.2 (YFP-Kv1.2), highly concentrated on axonal membranes (20), also increased the maximal spiking frequency compared with control, but much less compared with Kv3.1bHA (Fig. 2*A*). YFP-tagged Kv4.2 (YFP-Kv4.2), concentrated on somatodendritic membranes, did not increase the spiking frequency at all (Fig. 2*A*). Expressing Kv3.1aHA also increased the maximal spiking frequency, but surprisingly the increase was markedly less compared with Kv3.1bHA (Fig. 2*A*). For a single AP, Kv3.1aHA and Kv3.bHA significantly shortened the AP duration and increased the afterhyperpolarization compared with YFP-Kv1.2 and YFP-Kv4.2 (Fig. 2, *B* and *D*). None of the channel constructs significantly affected the resting membrane potential (Fig. 2*C*). The resting membrane potentials for E18 neurons (7–10 DIV, −60.73 ± 0.83 mV, $n = 48$; 14–16 DIV, −62.47 ± 0.90 mV, $n = 19$) and P8 neurons (14–16 DIV, −60.78 ± 0.68 mV, $n = 49$) under our experimental conditions were similar. Neither Kv3.1aHA nor Kv3.1bHA expression changed inward NaV currents in hippocampal neurons (supplemental Fig. S3). Detailed analysis of the input-output relationship showed Kv3.1bHA was significantly more effective in increasing the maximal spiking frequency compared with Kv3.1aHA (Fig. 2*E*). In contrast, both Kv3.1aHA and Kv3.1bHA enabled young neurons to follow high-frequency inputs (Fig. 2, *F* and *G*, and supplemental Fig. S4).

Biophysical Properties of Kv Channel Constructs—To understand why these channels differentially altered the neuronal firing frequency, we examined their biophysical properties by performing voltage-clamp recordings on transfected HEK293 cells. Due to the space clamp problem, it is difficult to accurately determine channel biophysical properties using whole cell recording on neurons. When expressed in HEK293 cells, the four constructs gave large currents (~10 nA) compared with the small endogenous current (~0.2 nA) (Fig. 3, *A* and *B*). Detailed biophysical properties of HA-tagged Kv3.1 channels, Kv3.1aHA and Kv3.1bHA, were not examined before. Although untagged Kv1.2 and Kv4.2 only carried much smaller currents (1–3 nA) when expressed in HEK293 cells, YFP-tagged Kv1.2 and Kv4.2 gave large currents comparable with Kv3.1aHA and Kv3.1bHA, most likely due to different expression levels. However, YFP fusion may alter the channel property. Therefore, it is important to determine their biophysical properties. Kv3.1aHA and Kv3.1bHA displayed identical channel properties, includ-

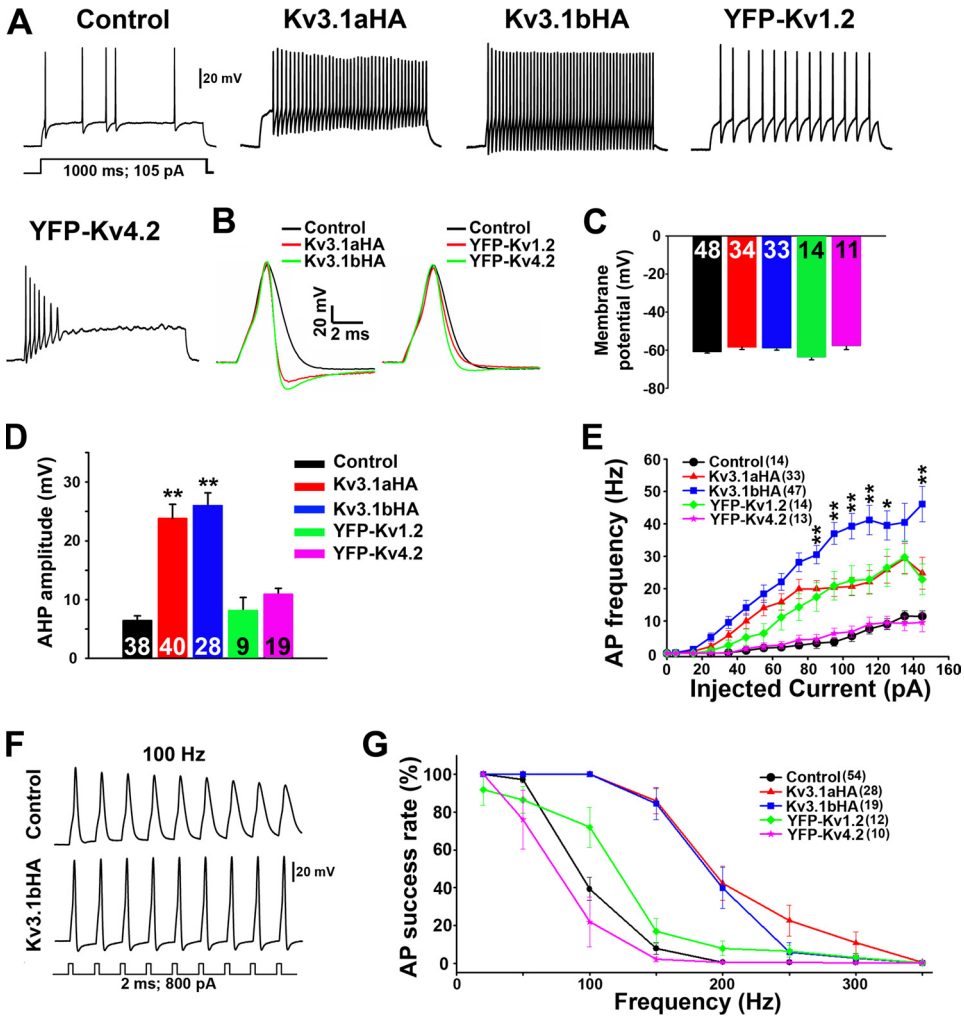

FIGURE 2. **Expression of Kv3.1b effectively converts slow-spiking neurons to fast-spiking ones.** *A,* overexpression of Kv3.1bHA or Kv3.1aHA significantly increased firing frequencies of APs induced by long-pulse current injections. Hippocampal neurons transfected with YFP (as control), Kv3.1aHA + YFP (indicator for transfection), Kv3.1bHA + YFP, YFP-Kv1.2, or YFP-Kv4.2 were examined with whole cell recording. Currents with 1000-ms duration and 10-pA increments from 5 to 145 pA were injected to the neuronal soma through the recording electrode. An example trace of APs induced by 105 pA current is shown for each condition. *B,* example waveforms of APs recorded from the neurons expressing different Kv channel constructs. *C,* resting membrane potentials of transfected neurons. *D,* average amplitude of after-hyperpolarization potential (*AHP*) of the transfected neurons. One-way analysis of variance followed by a Dunn test, **, $p < 0.01$. *E,* relationship of injected current and AP firing frequency in neurons expressing different Kv channels, between Kv3.1aHA and the Kv3.1bHA *t* test: **, $p < 0.01$; *, $p < 0.05$. The *p* values were adjusted by the Holm-Bonferroni method from repeat measures of Kv3.1bHA. *F,* APs induced by short-pulse current injections from a control neuron and a Kv3.1bHA-expressing neuron. Short current pulses (2 ms; 800 pA) with 100 Hz frequency were injected into the neuronal soma. *G,* relationship of the frequency of short-pulse current injections and AP success rate. The "*n*" numbers are provided in *parentheses*.

ing their activation threshold (about −20 mV), conductance-voltage relationship, activation (Kv3.1aHA τ_{on}, 0.20 ± 0.02 ms; Kv3.1bHA τ_{on}, 0.22 ± 0.01 ms), and deactivation (Kv3.1aHA τ_{off}, 0.65 ± 0.11 ms; Kv3.1bHA τ_{off}, 0.74 ± 0.03 ms) time constants (Fig. 3). This is consistent with previously published results (13, 16, 28). In contrast, YFP-Kv1.2 and YFP-Kv4.2 had very different channel properties. YFP-Kv1.2 was activated around −20 mV (YFP fusion may increase the activation threshold of Kv1.2), similar to Kv3.1aHA and Kv3.1bHA, whereas YFP-Kv4.2 was activated around −40 mV and displayed clear inactivation (Fig. 3, *A* and *E*). Importantly, both YFP-Kv1.2 (τ_{on}, 2.88 ± 0.30 ms; τ_{off}, 2.79 ± 0.11 ms) and YFP-Kv4.2 (τ_{on}, 0.74 ± 0.04 ms; τ_{off}, 6.34 ± 0.20 ms) activated and deactivated much slower compared with Kv3.1 channels (Fig. 3, *C*, *D*, and *F*), consistent with previous studies (43–46). The differences indicate why YFP-Kv1.2 and YFP-Kv4.2 expression did not markedly increase the spiking frequency as Kv3.1bHA did. However, our data have raised a very interesting question. Why do Kv3.1bHA and Kv3.1aHA have identical channel biophysical properties but differentially regulate the spiking frequency?

The Mechanism Underlying Kv3.1 Axonal Targeting and Its Impact on Spiking Frequency—We wondered whether the polarized targeting of Kv3.1 channels plays an important role in regulating the spiking frequency. Two splice variants of Kv3.1, Kv3.1a and Kv3.1b, differ in their polarized axon-dendrite targeting (16). Whereas Kv3.1a is restricted on somatodendritic membranes, Kv3.1b is more enriched on axonal membranes (16). To determine the impact of channel targeting on spiking frequency, we first made Kv3.1 channel mutants with unchanged channel activity but altered targeting. Our protein biochemistry and cell biology studies suggest that the splice

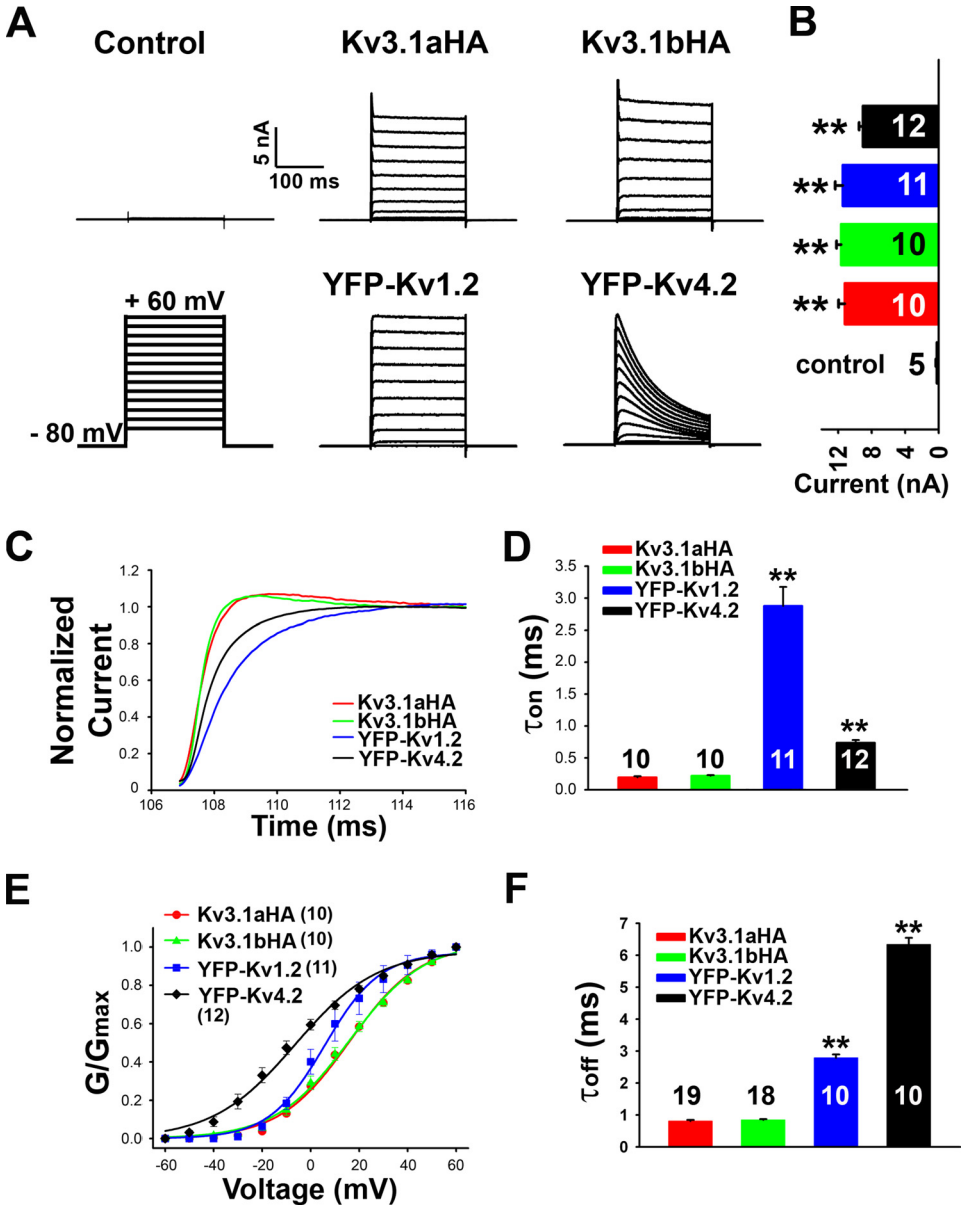

FIGURE 3. **Biophysical properties of different Kv channel constructs.** *A*, whole cell voltage-clamp recording was performed on HEK293 cells transfected with Kv3.1aHA, Kv3.1bHA, YFP-Kv1.2 (Kvβ2 was co-transfected to enhance the channel expression), or YFP-Kv4.2. Membrane potentials of cells were held at −80 mV and voltage pulses were applied from −60 to +60 mV with 10-mV increments (*lower left*). *B*, current amplitudes of different Kv channel constructs expressed in HEK293 cells are provided in mean ± S.E. Control cells expressing YFP, 0.24 ± 0.08 nA; Kv3.1aHA (*red*), 11.22 ± 0.74 nA; Kv3.1bHA (*green*), 11.66 ± 0.55 nA; YFP-Kv1.2 (*blue*), 11.47 ± 0.89 nA; YFP-Kv4.2 (*black*), 9.05 ± 0.46 nA. The "*n*" numbers are provided. *C*, the initial rising phase of channel currents recorded at +30 mV. *D*, activation time constant (τ_{on}) of different channel constructs. One-way analysis of variance followed by a Dunn test, **, $p < 0.01$. *E*, conductance and voltage curves of overexpressed Kv3.1aHA, Kv3.1bHA, YFP-Kv1.2, and YFP-Kv4.2 channels. *F*, deactivation time constant (τ_{off}) of different channel constructs. One-way analysis of variance followed by Dunn test, **, $p < 0.01$.

domain regulates the N/C-terminal interaction to expose the axonal targeting motif (ATM) in Kv3.1b (16), but how the splice domain carries out the regulation was not known. Thus, we made deletion constructs of Kv3.1b missing different portions of its C-terminal splice domain and examined their polarized axon-dendrite targeting (Fig. 4*A*). Whereas Kv3.1bHA$_{1-554}$ (F_{axon}/F_{dend}, 1.90 ± 0.14) and Kv3.1bHA$_{1-530}$ (F_{axon}/F_{dend}, 2.04 ± 0.11) were enriched on axonal membranes similar to Kv3.1bHA (F_{axon}/F_{dend}, 1.98 ± 0.11), Kv3.1bHA$_{1-513}$ (F_{axon}/F_{dend}, 0.26 ± 0.04) and Kv3.1bHA$_{1-502}$ (F_{axon}/F_{dend}, 0.35 ± 0.03) were contained on somatodendritic membranes similar to Kv3.1aHA (F_{axon}/F_{dend}, 0.27 ± 0.02) (Fig. 4, *A–E*, and supplemental Fig. S5). Therefore, the regulatory element of the splice domain most likely resides between residues 513 and 530 close to its N terminus (Fig. 4*A*).

Next, we determined the biophysical properties of channel deletion constructs using voltage-clamp recordings on transfected HEK293 cells. All deletion constructs except Kv3.1bHA$_{1-513}$ had unchanged channel properties compared with wild type Kv3.1bHA, including current amplitude, activation threshold, conductance-voltage relationship, and activation and deactivation time constants (supplemental Figs. S6 and S7). To determine their effects on spiking frequency, we transfected the three channel deletion constructs with

unchanged activity into neurons. Kv3.1bHA$_{1-513}$ and previously identified mutants at the ATM (16) had altered channel activity and therefore were not further examined for their impact on the spiking frequency (supplemental Fig. S7). Interestingly, Kv3.1bHA$_{1-554}$ and Kv3.1bHA$_{1-530}$ effectively enhanced the spiking frequency induced by prolonged current injection just like Kv3.1bHA, whereas Kv3.1bHA$_{1-502}$ functioned as Kv3.1aHA (Fig. 4*F* and supplemental Fig. S8*A*). No

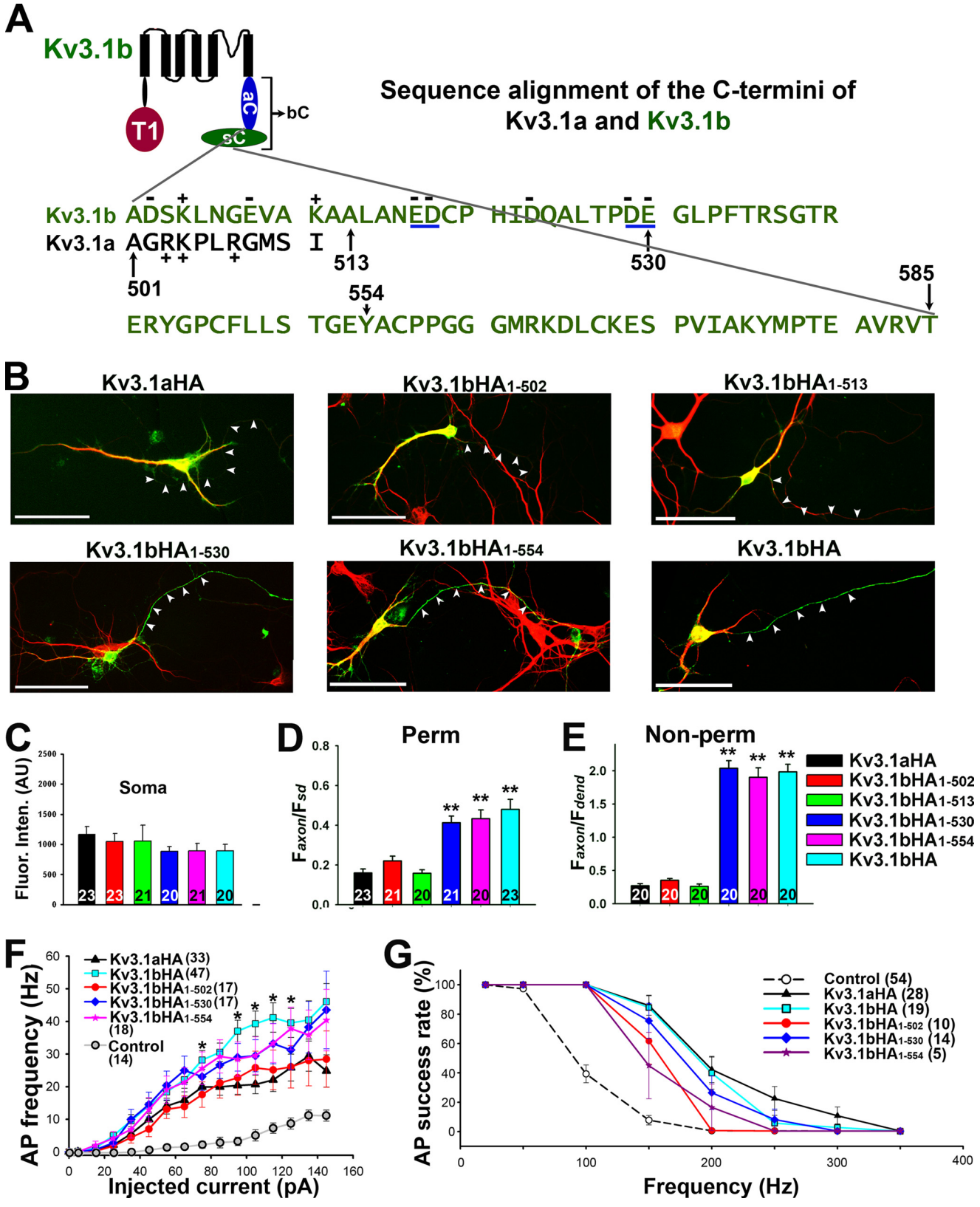

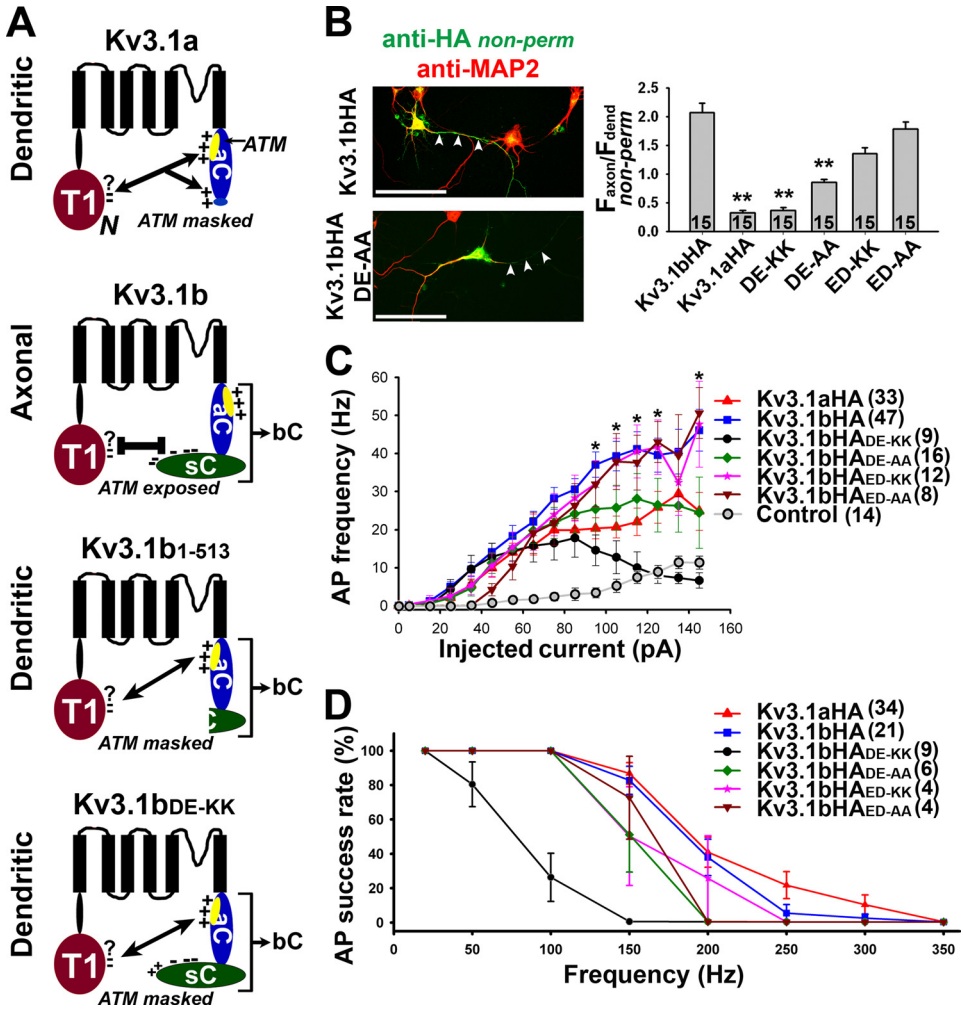

FIGURE 5. **Axonal targeting of Kv3.1b is critical for inducing the maximal AP firing frequency.** *A,* structure diagram of the role of charged residues of Kv3.1 splice domains in the N/C-terminal interaction and in exposing the ATM. *B,* the axon-dendrite targeting of Kv3.1b point mutants. Example images of Kv3.1bHA- and Kv3.1bHA$_{DE\text{-}AA}$-expressing neurons are on the *left*. The anti-HA staining (*green*) was performed under the nonpermeabilized condition. The anti-microtubule-associated protein 2 (*MAP2*) staining (*red*) labeled dendrites. *Scale bars*, 50 μm. Summary of the HA staining results are on the *right*. One-way analysis of variance followed by Dunnett's test, **, $p < 0.01$. *White arrowheads*, proximal axons. *C*, relationship of injected current and AP firing frequency, between Kv3.1bHA and Kv3.1bHA$_{DE\text{-}AA}$ *t* test: *, $p < 0.05$. The *p* values were adjusted by the Holm-Bonferroni method from repeat measures of Kv3.1bHA. *D*, success rate of action potentials induced by short-pulse current injection.

dramatic difference was observed among these channel constructs using the short-pulse current injection protocol (Fig. 4*G* and supplemental Fig. S8*B*). Therefore, these results support that axonal targeting of Kv3.1 channels significantly increases the spiking frequency. However, the truncation strategy cannot rule out the possibility that an unidentified binding protein to the deleted region of the splice domain may regulate channel activity.

After comparing the C termini of Kv3.1a and Kv3.1b, we found a striking difference, the net charge of the residues. The net charge between residues 501 and 530 in Kv3.1b is −5, whereas the net charge of the last 10 residues in Kv3.1a (residues 502–511) is +3 (Fig. 4*A*). Given the net charge of the C-terminal ATM is +8, we wondered if the electrostatic interaction plays an important role in the regulation of the N/C-terminal interaction by the splice domain, which may be essen-

FIGURE 4. **Regulation of axonal targeting and action potential firing by Kv3.1b truncations.** *A,* diagram of Kv3.1a and Kv3.1b C-terminal regions. Residues 1–501 are identical for the two splice variants. This region includes cytosolic N-terminal T1 domain (*red circle*), six membrane spanning segments (*6 black bars*), and the most part of cytosolic C terminus of Kv3.1a (*aC*). Kv3.1b has a large 85-residue splice domain (*sC*) at its C terminus. Thus, the Kv3.1b C terminus (*bC*) consists of aC and sC. Five numbers indicate positions of 5 residues. Within the N-terminal 30 residues, "minus" and "plus" indicate negatively and positively charged residues, respectively. *B,* cultured hippocampal neurons transfected with Kv3.1bHA deletion constructs at 5 DIV. The transfected neurons at 7 or 8 DIV were stained with an anti-HA antibody (*green*) under a nonpermeabilized condition and with an anti-microtubule-associated protein 2 (*MAP2*) antibody (*red*) under a permeabilized condition. *White arrowheads* indicate proximal axons. *Scale bars*, 100 μm. *C*, summary of the average fluorescence intensities of Kv3.1 constructs expressed in neuronal soma under the permeabilized condition. *D,* summary of axonal levels of the mutants stained under the permeabilized condition. One-way analysis of variance followed by Dunn test, **, $p < 0.01$. *E,* summary of polarized targeting of the mutants stained under a nonpermeabilized condition. One-way analysis of variance followed by Dunnett's test, **, $p < 0.01$. *F*, summary of the relationship of the amount of sustained injected current and AP firing frequency. Between Kv3.1bHA and Kv3.1bHA$_{1-502}$ *t* test: *, $p < 0.05$. The *p* values were adjusted by a Holm-Bonferroni method from repeat measures of Kv3.1bHA. The control is the same as in Fig. 2*E*. *G,* summary of firing frequency following the short-pulse and high frequency inputs.

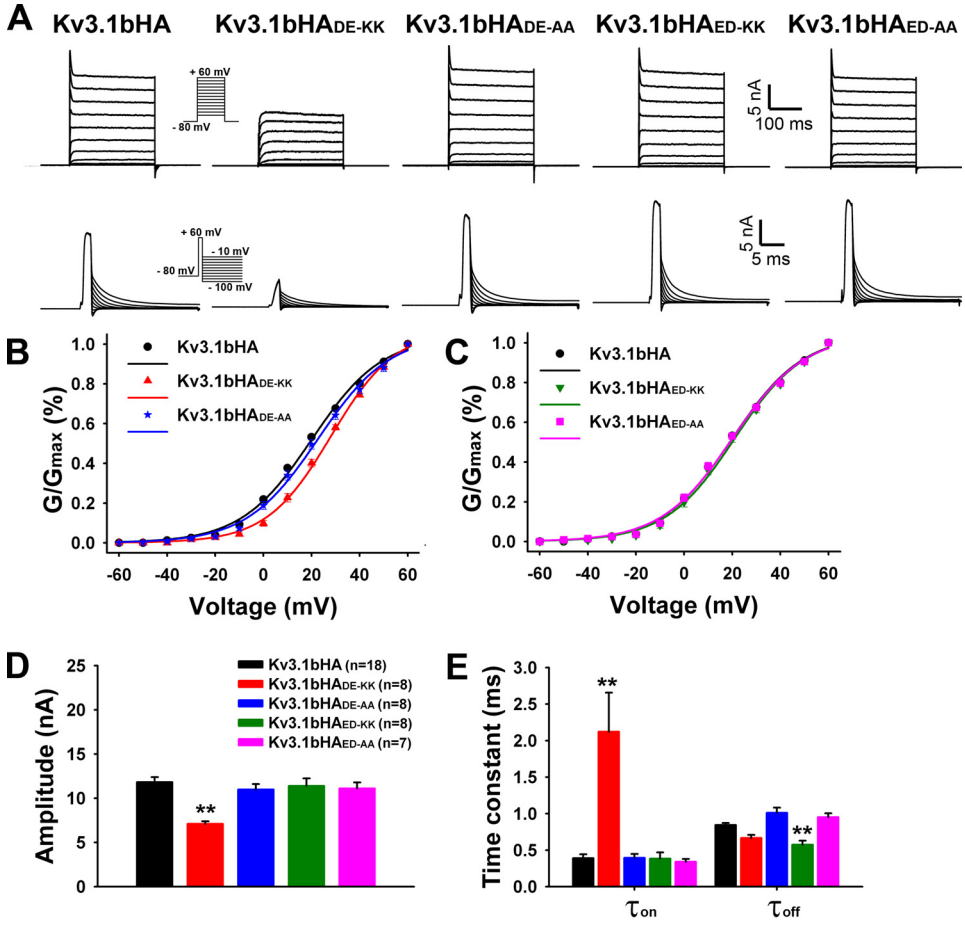

FIGURE 6. **Voltage-clamp recording of Kv3 channel constructs carrying point mutations.** *A*, current traces of voltage clamp recording. *B* and *C*, the G-V curves of Kv3.1bHA point mutations. *D*, current amplitudes of Kv3.1bHA point mutations. One-way analysis of variance followed by Dunnett's test, **, $p < 0.01$. *E*, activation (τ_{on}) and deactivation (τ_{off}) time constants of Kv3.1 channel constructs. One-way analysis of variance followed by Dunnett's test, **, $p < 0.01$.

tial in masking or unmasking the ATM (Fig. 5*A*). To test this hypothesis, we mutated two pairs of consecutive acidic residues in Kv3.1b to either two Lys or Ala residues. Interestingly, mutating D529E/D530E, Kv3.1bHA$_{DE\text{-}KK}$ (F_{axon}/F_{dend}, 0.37 ± 0.05), and Kv3.1bHA$_{DE\text{-}AA}$ (F_{axon}/F_{dend}, 0.85 ± 0.06), reduced axonal levels of Kv3.1bHA more significantly compared with mutating E517D/E518D, Kv3.1bHA$_{ED\text{-}KK}$ (F_{axon}/F_{dend}, 1.36 ± 0.10), and Kv3.1bHA$_{ED\text{-}AA}$ (F_{axon}/F_{dend}, 1.79 ± 0.12) (Fig. 5*B* and supplemental Fig. S9).

Next, we examined the effects of these point mutations on spiking frequency. The expression of Kv3.1bHA$_{DE\text{-}KK}$ failed to enhance the maximal firing frequency (Fig. 5, *C* and *D*). In sharp contrast, both Kv3.1bHA$_{ED\text{-}KK}$ and Kv3.1bHA$_{ED\text{-}AA}$ were similar to Kv3.1bHA in enhancing the maximal spiking frequency (Fig. 5, *C* and *D*). Interestingly, Kv3.1bHA$_{DE\text{-}AA}$, similar to Kv3.1aHA in targeting, did not markedly enhance the maximal spiking frequency as effectively as Kv3.1bHA (Fig. 5, *C* and *D*).

We further analyzed the channel biophysical properties of these mutants expressed in HEK293 cells. Kv3.1bHA$_{DE\text{-}KK}$ indeed had markedly smaller current and slower activation time constants, whereas the other three mutants had identical channel biophysical properties as the wild type Kv3.1bHA (Fig. 6). Taken together, our mutagenesis studies (Figs. 4–6) suggest that electrostatic attraction and repulsion of the splice domain to the N-terminal T1 domains regulate the masking and unmasking of the C-terminal ATM. The axonal targeting of Kv3.1 channels is critical for the maximal AP firing frequency.

Locally Blocking Kv3.1b in Proximal Axons but Not Dendrites Decreases the Spiking Frequency—To determine whether suppressing Kv3.1 channel activity on either axonal or dendritic membranes affects spiking frequency, we applied 1 mM TEA using a fine-opening glass pipette to the neurons expressing Kv3.1b and displaying fast spiking (Fig. 7*A*). When 1 mM TEA was applied to a large area including soma, as well as proximal dendrites and axon, the spiking frequency was markedly reduced and could partially recover after washing (control as 100%; TEA, 15.90 ± 3.89%; wash, 42.63 ± 19.78%) (Fig. 7, *B* and *G*). When TEA was applied to the proximal axon, the spiking frequency was also markedly reduced and the inhibitory effect was reversible (control as 100%; TEA, 46.50 ± 7.37%; wash, 89.87 ± 3.16%) (Fig. 7, *C*, *D*, and *G*). In contrast, the application of TEA at the proximal dendrite had no effect on the spiking frequency (control as 100%; TEA, 93.14 ± 3.13%; wash, 99.55 ± 4.74%) (Fig. 7, *E*–*G*). This result further supports our conclusion that Kv3.1 channels along the proximal axon, including the AIS, are the most critical for the fast spiking of neurons.

Simulations Reveal the Effect of Kv3 Polarized Targeting on Spiking Frequency—To further elucidate whether the axonal targeting of Kv3.1 channels is critical for fast spiking, we per-

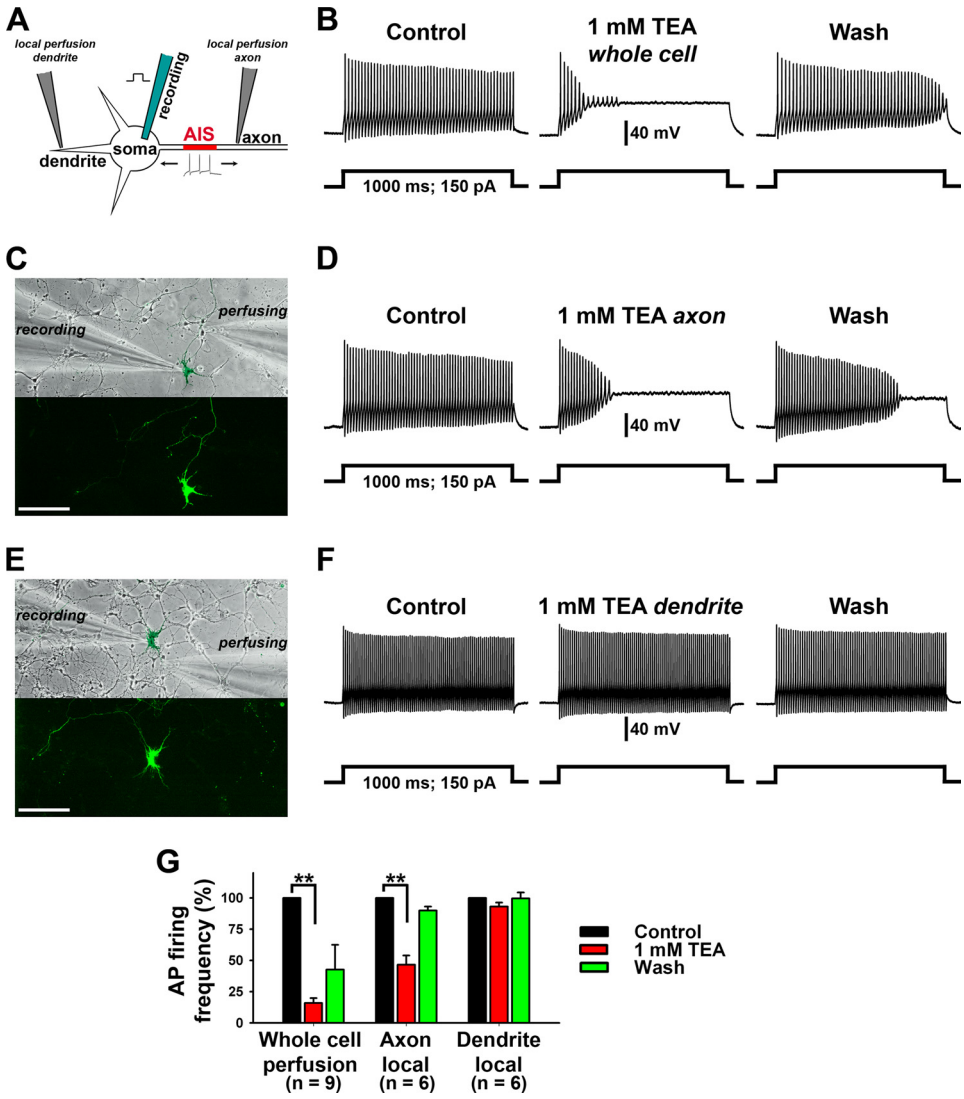

FIGURE 7. **Locally blocking axonal but not dendritic Kv3.1 channel activity reduced the firing frequency of APs induced by sustained depolarization.** *A,* diagram of whole cell current recording and local perfusion in axons or dendrites. *B*, the effect of TEA perfusion of the whole neuron on fast spiking of a Kv3.1bHA-transfected neuron. *C*, the effect of TEA local perfusion at the proximal axon of a Kv3.1bHA-transfected neuron. Images of local perfusion in proximal axons. *D*, APs induced in *C* were reversibly blocked by TEA local perfusion. *E*, images of local perfusion of dendrites. *F*, APs were unaffected in *E*. *G*, summary of TEA perfusion. *Scale bars*, 100 μm. Paired *t* test, **, $p < 0.01$.

formed simulation analysis. By using the NEURON software, we built three model neurons with identical geometry and NaV and leaky channel distribution, but with different amounts and localization of Kv3.1 channels. In the control neuron that has NaV channels at the AIS but no Kv3.1 channels, a simulated prolonged depolarization induced only a small number of APs (30 Hz with 150 pA current injected) (Fig. 8, *A* and *B*). In the dendritic Kv3.1 neuron that has Kv3.1 channels mainly enriched on somatodendritic membranes, a simulated depolarization induced more APs (80 Hz with 150 pA current injected) (Fig. 8, *A* and *B*). Importantly, in the axonal Kv3.1 neuron that has Kv3.1 channels enriched on axonal membranes, a simulated depolarization induced markedly more APs (110 Hz with 150 pA current injected) (Fig. 8, *A* and *B*). Qualitatively similar results were obtained with varied absolute values of current densities of NaV, Kv3.1, and leaky channels (see details under "Experimental Procedures"). Therefore, the simulation results suggest that Kv3.1 axonal targeting is a powerful means to increase the maximal spiking frequency, consistent with our experimental results.

DISCUSSION

In this study, we show that both biophysical properties and axonal targeting of Kv3.1 channels are critical to enable neurons to fire APs at the maximal frequency (Fig. 8*C*). We further reveal novel mechanistic insights into Kv3.1 axonal targeting, which includes electrostatic interactions between the N/C termini of the channel (Fig. 5*A*).

The maximal spiking frequency requires both rapid biophysical kinetics and axonal targeting. Blocking Kv3 effectively decreased the spiking frequency in both mature neurons and young neurons expressing Kv3.1bHA (Figs. 1 and 7), consistent with the critical role of Kv3 channels in fast-spiking neurons. The uniquely high activation threshold (about −20 mV, although other Kv channels about −40 mV) and fast deactivation kinetics (at least 10 times faster than other Kv

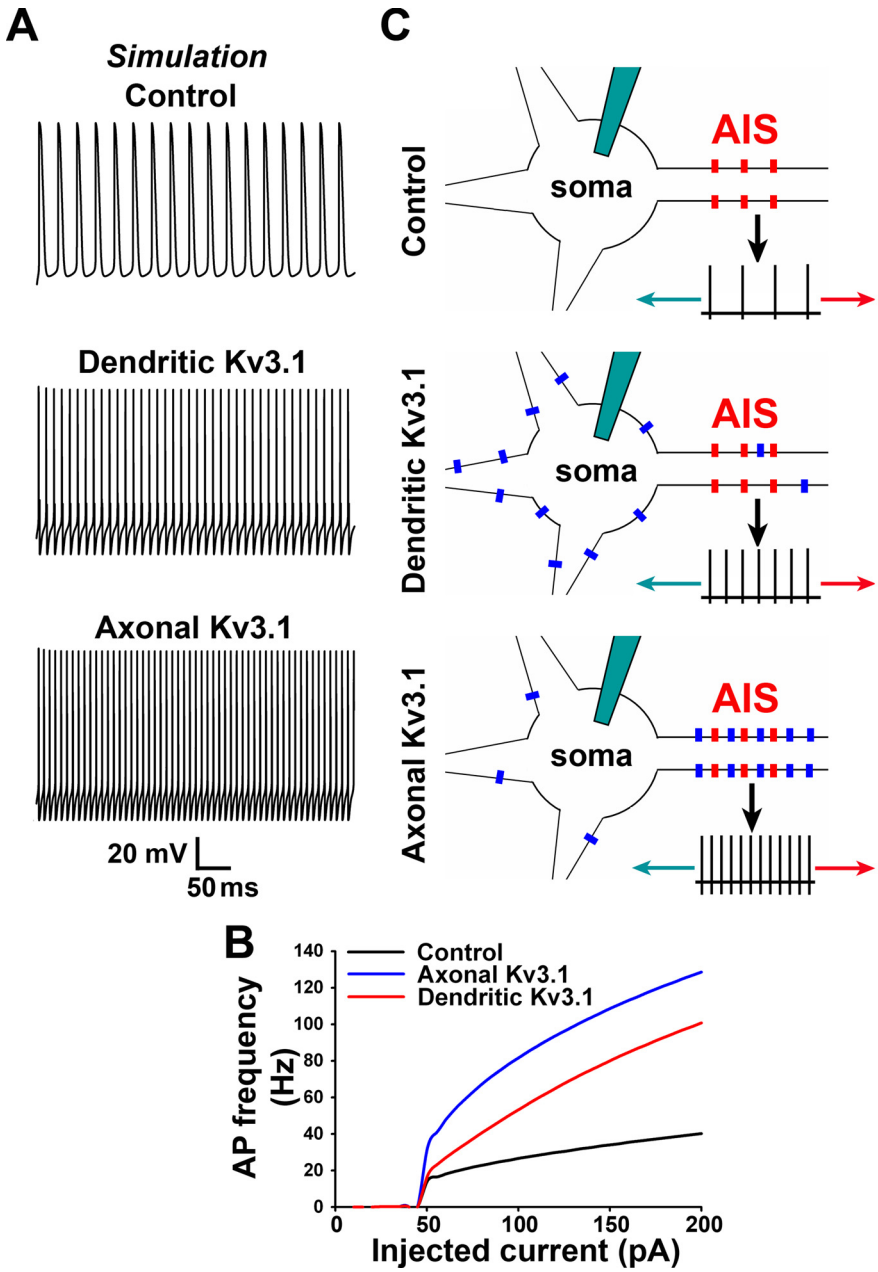

FIGURE 8. **Modeling and simulations of the effect of Kv3.1 axonal targeting on spiking frequency.** *A*, simulated action potential traces for neurons expressing no Kv3.1 (*top*), dendritic Kv3.1 (*middle*), and axonal Kv3.1 (*bottom*). *B*, the input-output relationship of the three simulated neurons. See "Experimental Procedures" for details of the parameter values. *C*, hypothetical models of a control neuron (*top*), a neuron expressing dendritic Kv3.1a (*middle*), and a neuron expressing axonal Kv3.1b (*bottom*). *Red bars*, NaV channels at the AIS; *blue bars*, Kv3.1 channels.

channels) of Kv3 channels are thought to be essential for fast spiking (28). Our results are consistent with this notion and further show that expression of axonal Kv3.1 channels is sufficient to induce fast spiking in young hippocampal neurons (Fig. 2). In sharp contrast, none of the neurons expressing YFP-Kv1.2 or YFP-Kv4.2 displayed fast spiking (Fig. 2), although both channels were expressed on plasma membranes (20, 22) and provided large outward currents (Fig. 3). Interestingly, YFP-Kv1.2 had a similar activation threshold with Kv3.1bHA, but much slower in activation and deactivation (Fig. 3). YFP-Kv1.2 expression did somewhat increase the spiking frequency, but never induced fast spiking (Fig. 2). Furthermore, a Kv3.1b mutant, Kv3.1bHA$_{DE\text{-}KK}$, displaying markedly increased activation time constant and threshold, but unaltered deactivation (Fig. 6), also failed to induce fast spiking (Fig. 5). Therefore, both activation and deactivation kinetics are critical for fast spiking. As expected, YFP-Kv4.2, displaying low activation threshold, and slow activation and deactivation kinetics (Fig. 3), did not increase the spiking frequency at all (Fig. 2).

Having the right channel biophysical properties alone is not sufficient for effective fast spiking. Kv3.1a has the same channel biophysical properties as Kv3.1b, but fails to induce fast spiking as effectively as Kv3.1bHA. The maximal range of spiking frequency requires axonal targeting of Kv3.1 channels, especially localization at the AIS. The channel density at the AIS was

much less for Kv3.1aHA (16). Furthermore, the Kv3.1bHA mutations, Kv3.1bHA$_{1-530}$, Kv3.1bHA$_{1-554}$, Kv3.1bHA$_{ED\text{-}KK}$, and Kv3.1bHA$_{ED\text{-}AA}$, with unchanged levels at the AIS can induce fast spiking, whereas the mutants, Kv3.1bHA$_{1-502}$ and Kv3.1bHA$_{DE\text{-}AA}$, with unchanged channel activity but decreased AIS levels, failed to effectively increase the maximal spiking frequency (Figs. 4 and 5). This result is consistent with our hypothesis. Furthermore, blocking Kv3.1 activity locally at proximal axons but not dendrites reduced fast spiking (Fig. 7), also supporting our hypothesis. Finally, simulations show that localization of Kv3 channels at the proximal axon including the AIS is critical for inducing the maximal spiking frequency (Fig. 8). Because APs are initiated at the AIS in most neurons, and this is where NaV channels are concentrated, the presence of Kv3.1 channels at the AIS allows them to more effectively regulate spiking frequency. Somatodendritic Kv3.1aHA still increases the spiking frequency; this may be due to either: 1) the electrical field passively spreading from the soma, or 2) low levels of Kv3.1aHA existing at the AIS. Nonetheless, because many K^+ channels have cytosolic ancillary subunits (47), we cannot rule out the possibility of an unidentified binding protein to differentially regulate channel activities of Kv3.1a and Kv3.1b in neurons.

Why was no significant difference observed between Kv3.1aHA- or Kv3.1bHA-expressing neurons when APs were induced by transient current injections? Both enabled neurons to follow high frequency stimulations (Fig. 2). Less Kv3.1 channel activity or an attenuated electrical field, provided by somatodendritic Kv3.1 channel activity, might be sufficient for transient stimulations. Alternatively, the protocol we used here may not be sensitive enough to detect the difference.

Both experimental data and computer simulations are consistent with the major conclusion that the axonal targeting of Kv3.1 channels regulates the maximal spiking frequency; however, there are minor differences between these two approaches. It is important to note that a native central neuron often expresses multiple types of voltage-gated ion channels, which may regulate the effectiveness of the function of the Kv3 channels in generating fast spiking. Our simulations were performed only with three types of channels: NaV, Kv3.1, and a leak (Fig. 8, *A* and *B*). The major conclusion of the simulations is that axonal Kv3.1 channels allow the neuron to fire at higher frequencies than dendritic ones (Fig. 8, *A* and *B*); this is consistent with the experimental data (Figs. 2, *4*, *5*, and *7*). However, there are two differences between the experimental data and the simulations. First, the maximal spiking frequency for the axonal-Kv3.1-expressing neuron in the simulations is about 120 Hz (Fig. 8*B*), whereas it is less than 60 Hz on average, for Kv3.1bHA-expressing neurons (Fig. 2*E*). Second, at the low spiking frequency, the effect of expressed Kv3.1bHA is not as strong as predicted by simulations. It is likely that smaller effects are difficult to show statistically in experimental results. More importantly, because, 1) Kv3.1 channels are activated at a higher membrane potential compared with Kv1, Kv2, and Kv4 channels and 2) the need for Kv channel activity to repolarize the membrane potential is less at the low current injection condition, the endogenous Kv currents may play a bigger role (supplemental Fig. S2). Recent studies show that AIS localization of NaV and calcium channels regulate AP initiation, waveform, and unidirectional propagation (48–52). Kv1 channels at the AIS of pyramidal neurons and interneurons regulate AP waveform and initiation (53, 54). How different channels at the AIS affecting different aspects of APs interact with the Kv3 channels functionally is an interesting question for future investigation.

Electrostatic interaction of the Kv3.1 N/C termini regulates polarized axon-dendrite targeting via exposing the ATM. Our previous studies suggested that the Kv3.1b splice domain weakens the masking effect of the N-terminal T1 domains onto the ATM. Subsequently, the exposed ATM is recognized by ankyrin G at the AIS and directs Kv3.1b targeting into axons (16). How the splice domain interferes with T1-ATM binding was not known. In the present study, using mutagenesis we have identified a novel electrostatic interaction of the Kv3.1 N/C termini interfered by the splice domain. First, using deletion analysis, we mapped the critical region in the splice domain from residues 513 to 530 (Fig. 4). This region (−5) and the last 10 residues of Kv3.1a (+3) are completely opposite in their net charges (Fig. 4*A*). Interestingly, the ATM in the C-terminal region had 8 positive net charges (16), which could mediate the masking effect by interacting with negative charges on the surface of the T1 domains, which contains a number of acidic residues. In Kv3.1a, the 3 positive charges of the C terminus may enhance T1-ATM binding to facilitate the masking effect of the ATM, whereas in Kv3.1b the negative charges within the splice domain repels the negatively charged T1 and weakens the masking of the ATM (Fig. 5*A*). The conclusion was supported by Kv3.1bHA point mutants (Figs. 5 and 6). This model, involving intramolecular interactions, is novel and deserves rigorous testing by other approaches in future studies, such as x-ray crystallography. Because we previously showed that the Kv3.1 N-/C-terminal interaction requires Zn^{2+}, the potential interaction of the splice domain and the Zn^{2+}-binding site is also an interesting question. Furthermore, the complex dynamic movement of membrane domains of Kv channels has been revealed (55). Our results that mutating D529E/D530E but not E517D/E518D affected Kv3.1bHA axonal targeting suggests an important role of conformational change(s), in addition to the electrostatic interaction, during the N-/C-terminal interaction and exposure of the ATM. This result is also consistent with a recent study showing the complex binding surfaces of the N-/C-terminal interaction in Kir2.1 channels (56).

Altering the spiking frequency via regulating Kv3 polarized targeting may underlie important physiological functions. Kv3-mediated fast spiking is critical for sensory and reflex functions in the central nervous system, for instance, in the sound location by the auditory circuit and in stabilizing images on the retina by the vestibule-ocular reflex circuit (57–59). Fast-spiking GABAergic interneurons in the hippocampus and cortex play important roles in learning and memory, and are implicated in epilepsy, schizophrenia, and drug addiction (38, 60). Prolonged and transient alteration of the spiking frequency can lead to profound physiological consequences. Regulation of the levels of Kv3 channel proteins and phosphorylation has been proposed as an underlying mechanism in adjusting the spiking frequency of neurons in the suprachiasmatic nucleus and auditory circuits following the circadian rhythm and different

acoustic environments, respectively (34, 61). In this study, we show that Kv3.1 channel protein targeting is a novel strategy for regulating spiking frequency, which may be the basis for development-regulated firing rates. The expression of two splice variants of Kv3.1, Kv3.1a and Kv3.1b, is developmentally regulated (62). As a result, with neuronal maturation, dendritic Kv3.1 channels shifts to axonal ones (23) to enhance the spiking frequency. In future studies, it is of interest to identify the potential activity-dependent regulation of neuronal spiking via altering Kv3 polarized targeting.

Acknowledgments—We thank Dr. C. Shrestha for technical assistance, Dr. L. Wei for advice on statistical analysis, and the University of California, Davis-NIH NeuroMab facility (a nonprofit supplier) for the monoclonal anti-Kv3.1b antibody.

REFERENCES

1. Wang, H., Kunkel, D. D., Martin, T. M., Schwartzkroin, P. A., and Tempel, B. L. (1993) Heteromultimeric K+ channels in terminal and juxtaparanodal regions of neurons. *Nature* **365,** 75–79
2. Sheng, M., Tsaur, M. L., Jan, Y. N., and Jan, L. Y. (1992) Subcellular segregation of two A-type K+ channel proteins in rat central neurons. *Neuron* **9,** 271–284
3. Rasband, M. N., Trimmer, J. S., Schwarz, T. L., Levinson, S. R., Ellisman, M. H., Schachner, M., and Shrager, P. (1998) Potassium channel distribution, clustering, and function in remyelinating rat axons. *J. Neurosci.* **18,** 36–47
4. Cooper, E. C., Milroy, A., Jan, Y. N., Jan, L. Y., and Lowenstein, D. H. (1998) Presynaptic localization of Kv1.4-containing A-type potassium channels near excitatory synapses in the hippocampus. *J. Neurosci.* **18,** 965–974
5. Veh, R. W., Lichtinghagen, R., Sewing, S., Wunder, F., Grumbach, I. M., and Pongs, O. (1995) Immunohistochemical localization of five members of the Kv1 channel subunits: contrasting subcellular locations and neuron-specific co-localizations in rat brain. *Eur. J. Neurosci.* **7,** 2189–2205
6. Monaghan, M. M., Trimmer, J. S., and Rhodes, K. J. (2001) Experimental localization of Kv1 family voltage-gated K+ channel alpha and beta subunits in rat hippocampal formation. *J. Neurosci.* **21,** 5973–5983
7. Trimmer, J. S. (1991) Immunological identification and characterization of a delayed rectifier K+ channel polypeptide in rat brain. *Proc. Natl. Acad. Sci. U.S.A.* **88,** 10764–10768
8. Du, J., Tao-Cheng, J. H., Zerfas, P., and McBain, C. J. (1998) The K+ channel, Kv2.1, is apposed to astrocytic processes and is associated with inhibitory postsynaptic membranes in hippocampal and cortical principal neurons and inhibitory interneurons. *Neuroscience* **84,** 37–48
9. Hwang, P. M., Cunningham, A. M., Peng, Y. W., and Snyder, S. H. (1993) CDRK and DRK1 K+ channels have contrasting localizations in sensory systems. *Neuroscience* **55,** 613–620
10. Trimmer, J. S., and Rhodes, K. J. (2004) Localization of voltage-gated ion channels in mammalian brain. *Annu. Rev. Physiol.* **66,** 477–519
11. Chow, A., Erisir, A., Farb, C., Nadal, M. S., Ozaita, A., Lau, D., Welker, E., and Rudy, B. (1999) K(+) channel expression distinguishes subpopulations of parvalbumin- and somatostatin-containing neocortical interneurons. *J. Neurosci.* **19,** 9332–9345
12. Goldberg, E. M., Watanabe, S., Chang, S. Y., Joho, R. H., Huang, Z. J., Leonard, C. S., and Rudy, B. (2005) Specific functions of synaptically localized potassium channels in synaptic transmission at the neocortical GABAergic fast-spiking cell synapse. *J. Neurosci.* **25,** 5230–5235
13. Ozaita, A., Martone, M. E., Ellisman, M. H., and Rudy, B. (2002) Differential subcellular localization of the two alternatively spliced isoforms of the Kv3.1 potassium channel subunit in brain. *J. Neurophysiol.* **88,** 394–408
14. Ishikawa, T., Nakamura, Y., Saitoh, N., Li, W. B., Iwasaki, S., and Takahashi, T. (2003) Distinct roles of Kv1 and Kv3 potassium channels at the calyx of Held presynaptic terminal. *J. Neurosci.* **23,** 10445–10453
15. Brooke, R. E., Atkinson, L., Batten, T. F., Deuchars, S. A., and Deuchars, J. (2004) Association of potassium channel Kv3.4 subunits with pre- and post-synaptic structures in brainstem and spinal cord. *Neuroscience* **126,** 1001–1010
16. Xu, M., Cao, R., Xiao, R., Zhu, M. X., and Gu, C. (2007) The axon-dendrite targeting of Kv3 (Shaw) channels is determined by a targeting motif that associates with the T1 domain and ankyrin G. *J. Neurosci.* **27,** 14158–14170
17. Chang, S. Y., Zagha, E., Kwon, E. S., Ozaita, A., Bobik, M., Martone, M. E., Ellisman, M. H., Heintz, N., and Rudy, B. (2007) Distribution of Kv3.3 potassium channel subunits in distinct neuronal populations of mouse brain. *J. Comp. Neurol.* **502,** 953–972
18. Martina, M., Yao, G. L., and Bean, B. P. (2003) Properties and functional role of voltage-dependent potassium channels in dendrites of rat cerebellar Purkinje neurons. *J. Neurosci.* **23,** 5698–5707
19. Johnston, J., Forsythe, I. D., and Kopp-Scheinpflug, C. (2010) Going native: voltage-gated potassium channels controlling neuronal excitability. *J. Physiol.* **588,** 3187–3200
20. Gu, C., Jan, Y. N., and Jan, L. Y. (2003) A conserved domain in axonal targeting of Kv1 (Shaker) voltage-gated potassium channels. *Science* **301,** 646–649
21. Gu, C., Zhou, W., Puthenveedu, M. A., Xu, M., Jan, Y. N., and Jan, L. Y. (2006) The microtubule plus-end tracking protein EB1 is required for Kv1 voltage-gated K+ channel axonal targeting. *Neuron* **52,** 803–816
22. Rivera, J. F., Ahmad, S., Quick, M. W., Liman, E. R., and Arnold, D. B. (2003) An evolutionarily conserved dileucine motif in Shal K+ channels mediates dendritic targeting. *Nat. Neurosci.* **6,** 243–250
23. Xu, M., Gu, Y., Barry, J., and Gu, C. (2010) Kinesin I transports tetramerized Kv3 channels through the axon initial segment via direct binding. *J. Neurosci.* **30,** 15987–16001
24. Lim, S. T., Antonucci, D. E., Scannevin, R. H., and Trimmer, J. S. (2000) A novel targeting signal for proximal clustering of the Kv2.1 K+ channel in hippocampal neurons. *Neuron* **25,** 385–397
25. Gu, C., and Barry, J. (2011) Function and mechanism of axonal targeting of voltage-sensitive potassium channels. *Prog. Neurobiol.* **94,** 115–132
26. Winckler, B., Forscher, P., and Mellman, I. (1999) A diffusion barrier maintains distribution of membrane proteins in polarized neurons. *Nature* **397,** 698–701
27. Song, A. H., Wang, D., Chen, G., Li, Y., Luo, J., Duan, S., and Poo, M. M. (2009) A selective filter for cytoplasmic transport at the axon initial segment. *Cell* **136,** 1148–1160
28. Rudy, B., and McBain, C. J. (2001) Kv3 channels: voltage-gated K+ channels designed for high-frequency repetitive firing. *Trends Neurosci.* **24,** 517–526
29. Bean, B. P. (2007) The action potential in mammalian central neurons. *Nat. Rev. Neurosci.* **8,** 451–465
30. Craig, A. M., and Banker, G. (1994) Neuronal polarity. *Annu. Rev. Neurosci.* **17,** 267–310
31. Horton, A. C., and Ehlers, M. D. (2003) Neuronal polarity and trafficking. *Neuron* **40,** 277–295
32. Kaech, S., and Banker, G. (2006) Culturing hippocampal neurons. *Nat. Protoc.* **1,** 2406–2415
33. Atzori, M., Lau, D., Tansey, E. P., Chow, A., Ozaita, A., Rudy, B., and McBain, C. J. (2000) H2 histamine receptor-phosphorylation of Kv3.2 modulates interneuron fast spiking. *Nat. Neurosci.* **3,** 791–798
34. Song, P., Yang, Y., Barnes-Davies, M., Bhattacharjee, A., Hamann, M., Forsythe, I. D., Oliver, D. L., and Kaczmarek, L. K. (2005) Acoustic environment determines phosphorylation state of the Kv3.1 potassium channel in auditory neurons. *Nat. Neurosci.* **8,** 1335–1342
35. Yang, B., Desai, R., and Kaczmarek, L. K. (2007) Slack and Slick K(Na) channels regulate the accuracy of timing of auditory neurons. *J. Neurosci.* **27,** 2617–2627
36. Hines, M. L., and Carnevale, N. T. (1997) The NEURON simulation environment. *Neural. Comput.* **9,** 1179–1209
37. Golomb, D., Donner, K., Shacham, L., Shlosberg, D., Amitai, Y., and Hansel, D. (2007) Mechanisms of firing patterns in fast-spiking cortical interneurons. *PLoS Comput. Biol.* **3,** e156
38. Bartos, M., Vida, I., and Jonas, P. (2007) Synaptic mechanisms of synchronized gamma oscillations in inhibitory interneuron networks. *Nat. Rev.*

Neurosci. **8,** 45–56
39. Baccaglini, P. I., and Spitzer, N. C. (1977) Developmental changes in the inward current of the action potential of Rohon-Beard neurones. *J. Physiol.* **271,** 93–117
40. Harris, G. L., Henderson, L. P., and Spitzer, N. C. (1988) Changes in densities and kinetics of delayed rectifier potassium channels during neuronal differentiation. *Neuron* **1,** 739–750
41. Gurantz, D., Ribera, A. B., and Spitzer, N. C. (1996) Temporal regulation of Shaker- and Shab-like potassium channel gene expression in single embryonic spinal neurons during K+ current development. *J. Neurosci.* **16,** 3287–3295
42. Nakamura, Y., and Takahashi, T. (2007) Developmental changes in potassium currents at the rat calyx of Held presynaptic terminal. *J. Physiol.* **581,** 1101–1112
43. Coetzee, W. A., Amarillo, Y., Chiu, J., Chow, A., Lau, D., McCormack, T., Moreno, H., Nadal, M. S., Ozaita, A., Pountney, D., Saganich, M., Vega-Saenz de Miera, E., and Rudy, B. (1999) Molecular diversity of K+ channels. *Ann. N.Y. Acad. Sci.* **868,** 233–285
44. Varga, A. W., Yuan, L. L., Anderson, A. E., Schrader, L. A., Wu, G. Y., Gatchel, J. R., Johnston, D., and Sweatt, J. D. (2004) Calcium-calmodulin-dependent kinase II modulates Kv4.2 channel expression and upregulates neuronal A-type potassium currents. *J. Neurosci.* **24,** 3643–3654
45. Scannevin, R. H., Wang, K., Jow, F., Megules, J., Kopsco, D. C., Edris, W., Carroll, K. C., Lü, Q., Xu, W., Xu, Z., Katz, A. H., Olland, S., Lin, L., Taylor, M., Stahl, M., Malakian, K., Somers, W., Mosyak, L., Bowlby, M. R., Chanda, P., and Rhodes, K. J. (2004) Two N-terminal domains of Kv4 K(+) channels regulate binding to and modulation by KChIP1. *Neuron* **41,** 587–598
46. Guan, D., Horton, L. R., Armstrong, W. E., and Foehring, R. C. (2011) Postnatal development of A-type and Kv1- and Kv2-mediated potassium channel currents in neocortical pyramidal neurons. *J. Neurophysiol.* **105,** 2976–2988
47. Pongs, O., and Schwarz, J. R. (2010) Ancillary subunits associated with voltage-dependent K+ channels. *Physiol. Rev.* **90,** 755–796
48. Hu, W., Tian, C., Li, T., Yang, M., Hou, H., and Shu, Y. (2009) Distinct contributions of Na(v)1.6 and Na(v)1.2 in action potential initiation and backpropagation. *Nat. Neurosci.* **12,** 996–1002
49. Grubb, M. S., and Burrone, J. (2010) Activity-dependent relocation of the axon initial segment fine-tunes neuronal excitability. *Nature* **465,** 1070–1074
50. Kuba, H., Oichi, Y., and Ohmori, H. (2010) Presynaptic activity regulates Na(+) channel distribution at the axon initial segment. *Nature* **465,** 1075–1078
51. Lorincz, A., and Nusser, Z. (2008) Cell-type-dependent molecular composition of the axon initial segment. *J. Neurosci.* **28,** 14329–14340
52. Bender, K. J., and Trussell, L. O. (2009) Axon initial segment Ca2+ channels influence action potential generation and timing. *Neuron* **61,** 259–271
53. Kole, M. H., Letzkus, J. J., and Stuart, G. J. (2007) Axon initial segment Kv1 channels control axonal action potential waveform and synaptic efficacy. *Neuron* **55,** 633–647
54. Goldberg, E. M., Clark, B. D., Zagha, E., Nahmani, M., Erisir, A., and Rudy, B. (2008) K+ channels at the axon initial segment dampen near-threshold excitability of neocortical fast-spiking GABAergic interneurons. *Neuron* **58,** 387–400
55. Tombola, F., Pathak, M. M., and Isacoff, E. Y. (2006) How does voltage open an ion channel? *Annu. Rev. Cell Dev. Biol.* **22,** 23–52
56. Ma, D., Taneja, T. K., Hagen, B. M., Kim, B. Y., Ortega, B., Lederer, W. J., and Welling, P. A. (2011) Golgi export of the Kir2.1 channel is driven by a trafficking signal located within its tertiary structure. *Cell* **145,** 1102–1115
57. Parameshwaran, S., Carr, C. E., and Perney, T. M. (2001) Expression of the Kv3.1 potassium channel in the avian auditory brainstem. *J. Neurosci.* **21,** 485–494
58. von Hehn, C. A., Bhattacharjee, A., and Kaczmarek, L. K. (2004) Loss of Kv3.1 tonotopicity and alterations in cAMP response element-binding protein signaling in central auditory neurons of hearing impaired mice. *J. Neurosci.* **24,** 1936–1940
59. Gittis, A. H., Nelson, A. B., Thwin, M. T., Palop, J. J., and Kreitzer, A. C. (2010) Distinct roles of GABAergic interneurons in the regulation of striatal output pathways. *J. Neurosci.* **30,** 2223–2234
60. Lewis, D. A., Hashimoto, T., and Volk, D. W. (2005) Cortical inhibitory neurons and schizophrenia. *Nat. Rev. Neurosci.* **6,** 312–324
61. Itri, J. N., Michel, S., Vansteensel, M. J., Meijer, J. H., and Colwell, C. S. (2005) Fast delayed rectifier potassium current is required for circadian neural activity. *Nat. Neurosci.* **8,** 650–656
62. Perney, T. M., Marshall, J., Martin, K. A., Hockfield, S., and Kaczmarek, L. K. (1992) Expression of the mRNAs for the Kv3.1 potassium channel gene in the adult and developing rat brain. *J. Neurophysiol.* **68,** 756–766